Journal of Medicinal Chemistry

ARTICLE

pubs.acs.org/jmc

Design and Characterization of a Potent and Selective Dual ATP- and Substrate-Competitive Subnanomolar Bidentate c-Jun N-Terminal Kinase (JNK) Inhibitor

John L. Stebbins,[†,∥] Surya K. De,[†,∥] Petra Pavlickova,[†] Vida Chen,[†] Thomas Machleidt,[‡] Li-Hsing Chen,[†] Christian Kuntzen,[§] Shinichi Kitada,[†] Michael Karin,[§] and Maurizio Pellecchia*[,†]

[†]Infectious and Inflammatory Disease Center, Cancer Center, Sanford-Burnham Medical Research Institute, 10901 North Torrey Pines Road, La Jolla, California 92037, United States

[‡]Life Technologies, Discovery and ADMET Services, 501 Charmany Drive, Madison, Wisconsin 53719, United States

[§]Laboratory of Gene Regulation and Signal Transduction, School of Medicine, University of California at San Diego, 9500 Gilman Drive, MC0723, La Jolla, California 92093-0723, United States

Supporting Information

ABSTRACT: c-Jun N-terminal kinases (JNKs) represent valuable targets in the development of new therapies. Present on the surface of JNK is a binding pocket for substrates and the scaffolding protein JIP1 in close proximity to the ATP binding pocket. We propose that bidentate compounds linking the binding energies of weakly interacting ATP and substrate mimetics could result in potent and selective JNK inhibitors. We describe here a bidentate molecule, **19**, designed against JNK. **19** inhibits JNK kinase activity (IC_{50} = 18 nM; K_i = 1.5 nM) and JNK/substrate association in a displacement assay (IC_{50} = 46 nM; K_i = 2 nM). Our data demonstrate that **19** targets for the ATP and substrate-binding sites on JNK concurrently. Finally, compound **19** successfully inhibits JNK in a variety of cell-based experiments, as well as in vivo where it is shown to protect against Jo-2 induced liver damage and improve glucose tolerance in diabetic mice.

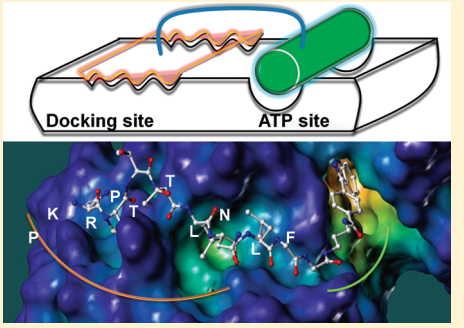

INTRODUCTION

The c-Jun N-terminal kinases (JNKs) are a series of serine/threonine protein kinases belonging to the mitogen activated protein kinase (MAPK) family. In mammalian cells, three distinct genes encoding JNKs have been identified, JNK1, JNK2, and JNK3, and at least 10 different isoforms exist.[1−3] JNK1, JNK2, and JNK3 share more than 90% amino acid sequence identity, and the ATP pocket is >98% homologous. JNK1 and JNK2 are ubiquitously expressed, whereas JNK3 is most commonly found in the brain, cardiac muscle, and testis.[2,4] JNK activation in response to stimuli such as stress or cytokines results in activation of several transcription factors and cellular substrates implicated in inflammation, insulin signaling, mRNA stabilization, and cell proliferation and survival.[3,5−7] Because of the link between these pathways and the pathogenesis of diseases such as Parkinson's and Alzheimer's and inflammatory diseases, cancer, diabetes, atherosclerosis, and stroke, JNK inhibitors are expected to be useful therapeutic agents.[1,3,8,9]

JNK binds to substrates and scaffold proteins, such as JIP-1, that contain a D-domain, as defined by the consensus sequence $R/K_{(2-3)}X_{(1-6)}L/I\text{-}X\text{-}L/I$.[10] A JIP1 D-domain peptide corresponding to amino acids 153−164, **20** (pepJIP1; sequence RPKRPTTLNLF; MW 1343), inhibits JNK activity in vitro and in cell while displaying extraordinary selectivity with negligible inhibition of the closely related MAP kinases p38 and Erk.[11−13] The mechanism of this inhibition is thought to be due to competition of **20** with the D-domains of JNK substrates or upstream kinases.[12,14] To increase stability and increase cell permeability of **20**, an all-D retro-inverso amino acid of compound **20** fused to the cell permeable HIV-TAT peptide, **11** (D-JNKI), was devised (sequence Ac-tdqsrpvqpflnlttprrprpprrrqrrkkrg-$CONH_2$; MW = 3395).[15] **11** significantly decreases c-Jun phosphorylation by JNK when tested in cell, however, albeit very selective, inhibition studies suggest that **11** is only a modest JNK inhibitor.[16] In comparison, the small molecule ATP mimetic, **21** (SP600125), is very potent in vitro but not very selective for JNK.[17−19] Hence, most of the current efforts focus on optimization of **21** and other ATP mimetics for the design of JNK inhibitors.[1,9,20]

Recently, using a combination of structure-based design guided by the X-ray structure of JNK1 in complex with **20** and **21**, as well as NMR fragment-based drug discovery approaches,[21] we proposed that by linking molecules that span these two sites we should be able to generate selective, high affinity bidentate JNK modulators. Indeed, we describe here a bidentate molecule with the

Received: April 20, 2011
Published: August 04, 2011

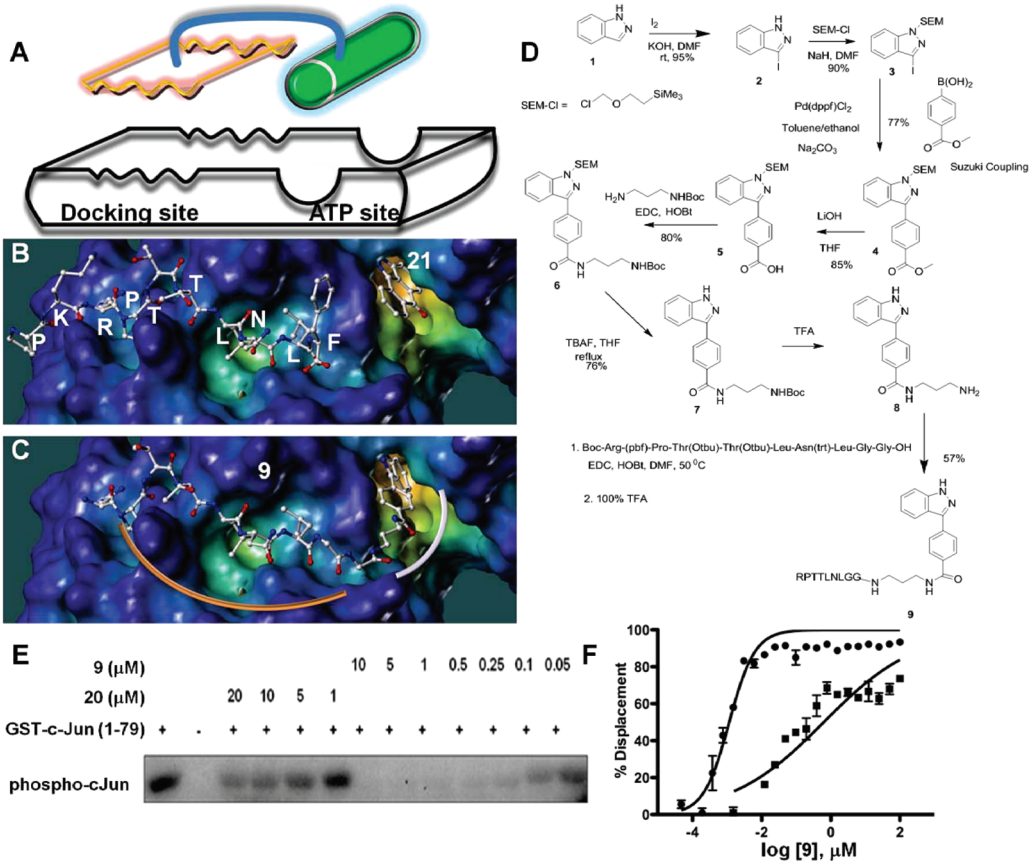

Figure 1. Fragment-based design and synthesis of bidentate JNK inhibitors. (A) Schematic representation of the proposed approach overlaid on the surface representation of JNK1 in complex with **20** (RPKRPTTLNLF) and the ATP mimic **21** (PDB-ID 1UKI). The surface generated with MOLCAD[50] and color coded according to cavity depth (blue, shallow; yellow, deep). (B) Docked structure of **20** and **21** on the surface of JNK1. (C) Docked structure of the bidentate compound **9** on the surface of JNK1. (D) Scheme for the synthesis of **8** and the bidentate **9** (see methods for experimental details). (E) In vitro JNK kinase activity inhibition by **9**. (F) Displacement of **20** from GST-JNK1 by **9** in absence (circles) and presence (squares) of a saturating amount of staurosporine (0.5 μM).

aforementioned characteristics that functions as a JNK inhibitor in vitro, in cell, and in a variety of in vivo models.

RESULTS AND DISCUSSION

In the realm of drug discovery, fragment-based drug design approaches are becoming increasingly successful in tackling challenging targets, such as those involving protein−protein interactions.[22] A common fragment-based drug design approach consists of designing bidentate compounds chemically linking two weakly interacting scaffolds that occupy adjacent pockets on the target's surface (Figure 1A−C). In this case, the free energy of binding of the resulting bidentate compound with respect to those of the individual fragments can be expressed as:

$$\Delta G^{AB} = \Delta H^{A} + \Delta H^{B} - T\Delta S^{AB}$$
$$= -RT\ln(K_D^{A} \times K_D^{B} \times E)$$

Where, R represents the Boltzmann constant, T is the temperature of the system, ΔH^{A} and ΔH^{B} are the enthalpy of binding of fragments A and B respectively, ΔS^{AB} represents the entropy loss upon binding of the bidentate compound, and $K_D{}^{A}$ and $K_D{}^{B}$ are the dissociation constants of the individual initial binders and E is the linking coefficient.[23] The recently determined X-ray structure of JNK1 in complex with **20** and the ATP-mimic **21**,[24] reveals a close proximity between the ATP and the docking binding sites, suggesting the possibility of obtaining high affinity and selective compounds by designing appropriate bidentate molecules. Indeed, this approach has been successfully executed for a variety of other proteins and kinases.[25−30] Hence, our hypothesis is that by tailoring a weak docking site binder to a weakly interacting ATP-mimic, it should be likewise possible to develop potent and selective inhibitors of JNK.

To define an optimal interacting docking peptide sequence for JNK we tested 20 peptide sequences derived from its putative substrates and scaffolding proteins, all presenting a D-domain consensus motif[10] (Supporting Information Table S1). Each peptide was tested for its ability to displace **20** (residues 153−164) from JNK1 by using a dissociation enhanced lanthanide fluoro-immuno assay (DELFIA) platform. DELFIA is a heterogeneous assay whereby a biotin-linked **20** is adsorbed onto a streptavidin-coated plate followed by incubation with GST-JNK1. Detection of the **20**/GST-JNK1 complex is facilitated by a highly fluorescent anti-GST Eu-antibody conjugate (Perkin−Elmer). On the basis of these data (Supporting Information Table S1), a minimal peptide sequence, **10** (RPTTLNL), was identified as necessary and sufficient to displace full-length **20** in this assay. We are confident that inhibition is not at the level of either GST or streptavidin as **10** did not significantly displace a previously described and unrelated binding pair (SIAH1/phyllopod peptide)[31] in a similar DELFIA assay platform when tested up to 45 μM.

dx.doi.org/10.1021/jm200479c |J. Med. Chem. 2011, 54, 6206–6214

Table 1. In Vitro Activity Data for Reported JNK Inhibitors

Molecule	ID (MW)	pepJIP Displacement	Kinase Inhibition
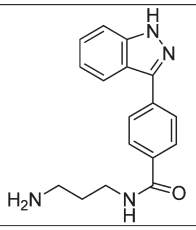	**8** (294)	IC_{50} = >50 μM	IC_{50} = 14 μM
Ac-RPTTLNL-OH	**10** (856)	IC_{50} = 4.5 μM	IC_{50} = >50 μM
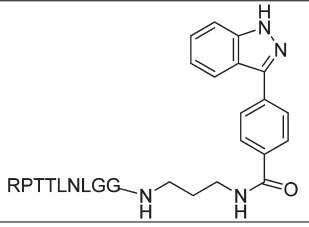	**9** (1236)	IC_{50} = 0.9 nM	IC_{50} = 0.7 nM
Ac-tdqsrpvqpflnlttprrprpprrrqrrkkrg-OH	**11** (3994)	IC_{50} = ~ 10 μM	IC_{50} = >50 μM
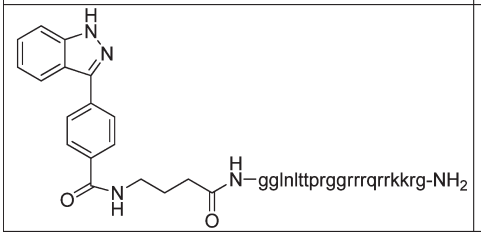	**19** (2728)	IC_{50} = 46 nM Ki = 1.5 nM	IC_{50} = 18 nM Ki = 2 nM

The design of a weak ATP mimetic JNK inhibitor was based on the structure of **21** (Figure 1B).[24] Given that **21** was found to potently inhibit several protein kinases,[17,18,20] in order to increase JNK selectivity and also facilitate subsequent synthetic efforts, we removed the keto group from **21**. Furthermore, on the basis of its docking mode, a convenient position to elongate the ATP-mimetic toward the docking site was identified in our previous work by using a combination of structure-based design guided by NMR-relaxation measurements using paramagnetic spin-labeling approaches.[21] These efforts resulted in the design of **8** (Figure 1D). The synthesis of **8** starts from the iodination of 1-azaindole with iodide and its protection with trimethylsilylethoxy methyl chloride, followed by a Suzuki coupling between 3 and 4-methoxycarbonylphenylboronic acid and attachment of the designed 3-carbon linker (Figure 1D).

8 is a relatively weak ATP mimetic, inhibiting JNK1 phosphorylation of the substrate ATF2 in the LanthaScreen time-resolved fluorescence resonance energy transfer (TR-FRET) based kinase activity assay (Invitrogen, Carlsbad, CA) with 14 μM IC_{50} value. Similarly, **10** was able to displace **20** in the DELFIA assay (IC_{50} 25 μM) but was unable to inhibit JNK1 phosphorylation of the substrate ATF2 in the same TR-FRET based kinase activity assay at concentrations up to 25 μM, hence representing a fairly weakly interacting substrate binding scaffold. However, when linked to the indazole moiety of **8**, the resulting compound **9** (Figure1D) was able to compete with **20** for JNK1 binding and inhibit JNK1 kinase activity with remarkable subnanomolar affinities (Table 1). To properly link compounds **8** and **10**, two Gly residues were inserted as part of the linker based on molecular modeling and NMR-based considerations and the X-ray structure of the ternary complex, as described in our previous studies.[21]

Consistent with the bidentate binding mode of **9** to JNK1, the preincubation of JNK1 with an excess of ATP-mimetic staurosporine,[32] thus eliminating one binding site, reduces the ability of **9** to compete with **20** binding to JNK1 by 600-fold (Figure 1F). As expected, under these circumstances, the IC_{50} for **9** was similar to that of the peptide alone (Table 1). Direct comparison of kinase inhibition properties of **9** (MW 1204) with **20** (MW 1343) clearly demonstrated an improvement of over 100-fold (Figure 1E). Hence, by linking the binding energy of a minimal **20** sequence with a modest **21** derived ATP mimetic, we successfully produced a very potent bidentate molecule representing a new class of JNK inhibitors.

To confer further favorable pharmacological properties to this compound for in vivo studies, analogous to the clinical candidate **11**,[16] we produced an all-D retro-inverso version of **9** fused to the cell penetrating HIV-TAT sequence. As expected, the resulting compound, **19** (Table 1), efficiently competes with **20** for binding to JNK1 as well as strongly inhibiting JNK1 kinase activity (Figure 2A, B), with IC_{50} values of 18 and 46 nM, respectively. Using the same in vitro kinase activity assay and the same ATF2 substrate, **19** was found to be inactive versus p38α at concentrations up to 100 μM, a member of the MAPK family with highest structural similarity to JNK, thus demonstrating selectivity. Lineweaver−Burk analysis indicates that **19** is competitive with both ATP and ATF2 for binding to JNK1 as the data with an apparent K(i) of 2 and 1.5 nM, respectively (Figure 2C,D). Consistent with the proposed bimodal binding of **19** to JNK1, the data fit very well with both the mixed and the

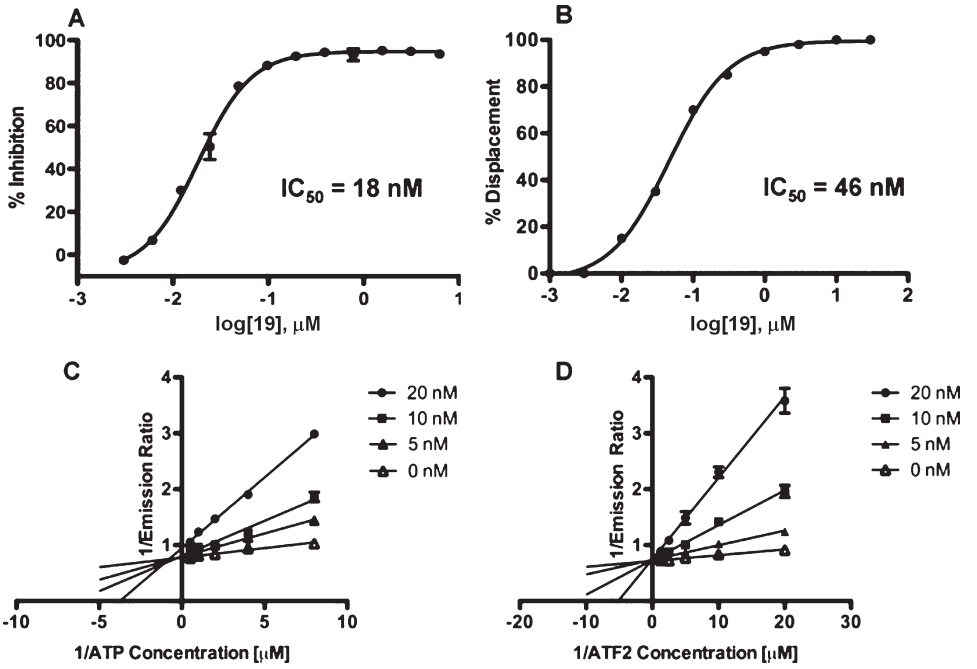

Figure 2. In vitro characterization of **19**. (A) Dose dependent displacement of biotinylated **20** from GST-JNK1 and (B) JNK kinase activity inhibition by **19**. (C and D) Lineweaver−Burk analysis with compound **19**.

competitive inhibition modes and very poorly with either the non-competitive or the uncompetitive inhibition models (Supporting Information Table S2).

In an attempt to further profile the biological properties of **19**, we compared its ability to function in the context of a complex cellular milieu with that of **11**. For this analysis, we employed a cell-based TR-FRET assay.[33] In this assay, **19** was significantly more effective at inhibiting tumor necrosis factor-α (TNF-α) stimulated phosphorylation of c-Jun in B16−F10 melanoma cells (EC_{50} = 14 μM), while both **11** and **21** were significantly less effective under the same experimental conditions (Figure 3A). The cell-based system employed makes use of a GFP-c-Jun stable expression system. As a result, the levels of GFP-c-Jun in these cells are higher than endogenous levels. This could have an inflationary effect on the EC_{50} values obtained with this assay when testing substrate competitive compounds. Thus, in an orthogonal assay, we measured the ability of **19** to inhibit anisomycin stimulated endogenous c-Jun phosphorylation in HEK293T cells. Indeed, we found 19 to be significantly more effective in this system (EC_{50} = 2 μM; Figure 3B). To further profile **19** efficacy in cell as well as demonstrate its selectivity, we tested the ability of **19** to inhibit the release of cytokines from RAW 264.7 mouse macrophage cells in response to lipopolysaccharide (LPS). LPS stimulated secretion of TNF-α from macrophages is dependent on JNK activation[34] whereas IL-1β secretion from RAW 264.7 cells is known to be p38 dependent.[35] We found that **19** was able to inhibit JNK dependent TNF-α release, while p38α dependent IL-1β secretion was unaffected (Figure 3C). Taken together, these findings conclusively establish that **19** as a potent and selective dual substrate and ATP competitive JNK bidentate inhibitor able to function efficiently and selectively in a cellular context.

JNK activation has been linked to the impaired glucose tolerance associated with type 2 diabetes.[8,36] Therefore we tested the ability of **19** to restore glucose tolerance in the type 2 diabetes mouse model NONcNZO10/LtJ[37] (Jackson Laboratories, Bar Harbor, Maine 04609, United States), chosen because obesity in NONcNZO10/LtJ mice reflects most human obesities. For this analysis, glucose intolerant NONcNZO10/LtJ mice were injected intraperitoneally daily for four days with 25 mg/kg **19**. The ability of mice to process glucose injected intraperitoneally was then measured. **19** was remarkably effective in restoring normoglycemia without inducing hypoglycemia compared to both the vehicle control and **11** (Figure 4A). The ability of **19** to improve glucose tolerance is consistent with its proposed function as an effective JNK inhibitor, while the observed shortcoming of compound **11** under our current experimental conditions can simply be a reflection of its limited potency against the target, as very recently corroborated by a comparative study.[38]

The link between hapototoxicity and JNK function has been established using JNK1−/− and JNK2−/− mice.[39−41] Thus, to extend our in vivo analysis of **19**, we tested its ability to block Jo2-induced liver damage as measured by the release of liver enzymes alanine-aminotransferase (ALT) and aspartate aminotransferase (AST) into the blood. **19** effectively blunted the Jo2-induced elevation of AST and ALT levels relative to control animals (Figure 4B). Consistent with its proposed ability to effectively inhibit JNK function in vivo, **19** treatment resulted in significantly reduced levels of phosphorylated c-Jun in the liver of treated mice as compared to the control (Figure 4C).

CONCLUSION

In conclusion, by applying the principles of fragment-based drug discovery to the design of dual ATP- and substrate-competitive kinase inhibitors, we identified bidentate molecules with superior JNK inhibitory properties. We anticipate that this approach will find wide applications in the design and synthesis of other potent and selective bidentate kinase inhibitors. Regarding the reported bidentate compounds, given that **11** is currently a clinical candidate (under XG102 by Xigen Corp., Lausanne, Switzerland), we can speculate that **19**, having markedly improved biochemical and pharmacological properties and even reduced

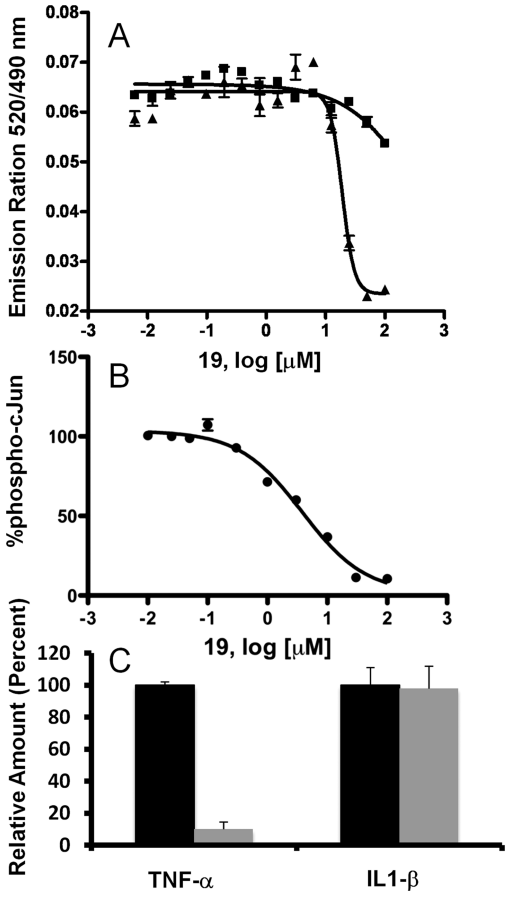

Figure 3. Cell-based characterization of **19**. (A) TR-FRET analysis of c-Jun phosphorylation upon TNF-α stimulation of B16−F10 cells in the presence of increasing **19** (closed triangles), **21** (inverted triangles) and **11** (closed squares). (B) Inhibitory effect of **19** on phospho-c-Jun upon anisomycin stimulation of HEK293T cell. (C) Compounds **19** and **11** effect on TNF-α and IL-1β levels after 5 h of exposure to LPS as compared to vehicle control. Results shown as percent of vehicle control ± SD ($n = 3$). Cytokine production was measured directly from cell culture medium by a sandwich immunoassay (Meso Scale Discovery).

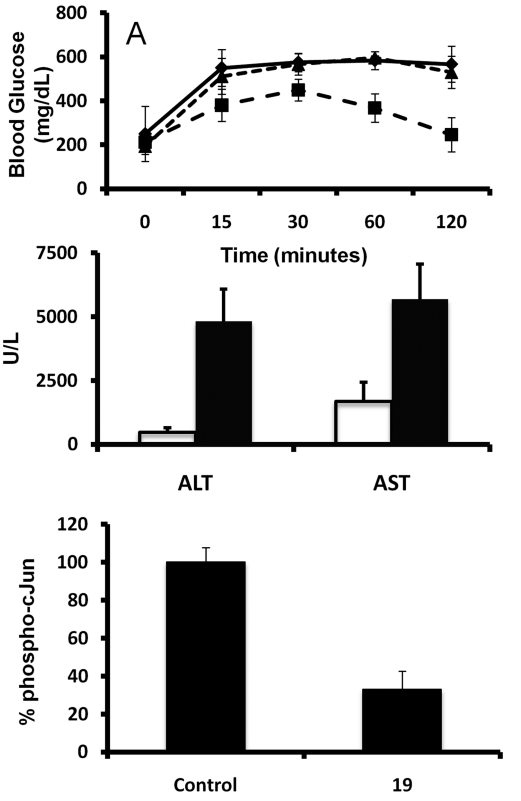

Figure 4. In vivo characterization of **19**. (A) Effect of **19** and **11** (25 mg/kg) on glucose tolerance in 26-week-old NONcNZO10/LtJ mice from Harlan (Jackson Laboratories, Bar Harbor, Maine 04609, United States). Solid diamonds, vehicle control; solid squares, 25 mg/kg **19**; solid triangle, 25 mg/kg **11**.). $p < 0.0001$ for the comparison of compound **19** with control, by two-way ANOVA using all the measurements. (B) Effect of 25 mg/kg **19** (open bars) on AST and ALT levels after Jo2 treatment as compared to vehicle control (filled bars). Data are mean ± SE for four mice. AST levels significantly different as compared to control mice $p < 0.05$. ALT levels significantly different as compared to control mice $p < 0.02$. (C) Effect of 25 mg/kg **19** on phospho-c-Jun levels in C57/B6 mouse liver. Phospho-c-Jun levels measured by sandwich immunoassay (Meso Scale Discovery). Results shown as percent of vehicle control ± SD ($n = 4$). $p <$ 0.0001 for the comparison of compound **19** with control, by unpaired t test.

molecular weight over **11**, could equally well enter further clinical investigations. Furthermore, our current efforts focused on the identification of small molecules **20** mimetics[42−45] could likewise lead, based on the reported results, to the design of additional bidentate compounds voided of the peptidyl nature.

Given the tremendous efforts of the past decade dedicated to the design of potent and selective kinase inhibitors for both therapeutics and basic cell biology studies, we are confident that the bidentate approach proposed will find wide applications in both the pharmaceutical and basic chemical biology arenas.

■ MATERIALS AND METHODS

DELFIA Assay (Dissociation Enhanced Lanthanide Fluoro-Immuno Assay). To each well of 96-well streptavidin-coated plates (Perkin-Elmer), 100 μL of a 100 ng/mL solution of biotin-labeled **20** (Biotin-lc-KRPKRPTTLNLF, where lc indicates a hydrocarbon chain of 6 methylene groups) was added. After 1 h incubation and elimination of unbound biotin-**20** by three washing steps, 87 μL of Eu-labeled anti-GST antibody solution (300 ng/mL; 1.9 nM), 2.5 μL DMSO solution containing test compound, and 10 μL solution of GST-JNK1 for a final protein concentration of 10 nM was added. After 1 h incubation at 0 °C, each well was washed five times to eliminate unbound protein and the Eu-antibody if displaced by a test compound. Subsequently, 200 μL of enhancement solution (Perkin-Elmer) was added to each well and fluorescence measured after 10 min incubation (excitation wavelength, 340 nm; emission wavelength, 615 nm). Controls include unlabeled peptide and blanks receiving no compounds. Protein and peptide solutions were prepared in DELFIA buffer (Perkin-Elmer). Staurosporine (Calbiochem; San Diego, CA; catalogue no. 569397) was included at 20-times molar equivalent GST-JNK1 and preincubated for 15 min on ice.

In Vitro Kinase Assay. Assay platform from Invitrogen was utilized. The time-resolved fluorescence resonance energy transfer assay (TR-FRET) was performed in 384-well plates. Each well received JNK1 (0.8 nM), ATF2 (200 nM), and ATP (1 μM) in 50 mM HEPES, 10 mM MgCl 2, 1 mM EGTA and 0.01% Brij-35, pH 7.5 and test compounds. The kinase reaction was performed at room temperature for 1 h. After this time, the terbium labeled antibody and EDTA were added into each well. After an additional hour incubation, the signal was measured at 520/495 nm emission ratio on a BMG Pherastar fluorescence plate reader.

dx.doi.org/10.1021/jm200479c |J. Med. Chem. 2011, 54, 6206–6214

Alternatively, **9** was kept as a 10 mM solution in 10% DMSO. Serial dilutions containing 1% DMSO were prepared and **9** was added at a ratio of 1:10 to each kinase reaction to obtain the indicated final concentrations. JNK kinase assays were performed with 50 ng per reaction of active JNK2α2 from Upstate/Millipore (catalogue no. 14−329) according to the recommendations of the manufacturer with the following changes: GST-c-Jun (1−79) was used as a substrate 1 μg per reaction.[46] The kinase reactions were performed at 30 °C for 20 min without Brij-35 and were stopped by addition of 2× Laemmli loading buffer and boiling for 3 min. The proteins were then separated on a mini gel and transferred to a PVDF membrane by wet blot. The membranes were dried and exposed to film.

Phospho-c-Jun Detection and Quantification. All cell culture media and supplements were from Life Technologies. The B16−F10 murine melanocyte cell line was purchased from ATCC and maintained according to manufacturers recommendations. At 48 h prior to measuring phospho-c-jun levels, cells were transduced with BacMam GFP−c-Jun (1−79). BacMam preparation and transductions were performed as previously reported.[47] Briefly, the cells were grown in 10 cm dishes to approximately 75% confluence. The transduction was performed by adding 10% vol/vol BacMam virus stock in combination with Trichstatin A at a final concentration of 0.5 mM. The cells were incubated for 24 h. BacMam GFP-c-Jun (1−79) transduction efficiency, as determined by fluorescence microscopy, exceeded in general 80% of the cell population. All transductions were performed at a signal saturating MOI (at least 500 IU/cell). Following the transduction, the cells were trypsinized and plated in white tissue culture treated 384-well plates at a density of 25000 cell per well in 32 mL of assay medium (Opti-MEM, supplemented with 0.1% charcoal/dextran-treated FBS, 100 U/mL penicillin and 100 mg/mL streptomycin, 0.1 mM nonessential amino acids, 1 mM sodium pyruvate, 25 mM HEPES pH 7.3, and lacking phenol red). After overnight incubation, cells were pretreated for 60 min with compound (indicated concentrations) followed by 30 min of stimulation with 2 ng/mL of TNF-α. The medium was then removed by aspiration, and the cells were lysed by adding 20 mL of lysis buffer (20 mM TRIS-HCl pH 7.6, 5 mM EDTA, 1% NP-40 substitute, 5 mM NaF, 150 mM NaCl, 1:100 protease and phosphatase inhibitor mix, SIGMA P8340 and P2850, respectively). The lysis buffer included 2 nM of the terbium labeled antipc-Jun (pSer73) detection antibody (Life Technologies). After allowing the assay to equilibrate for 1 h at room temperature, TR-FRET emission ratios were determined on a BMG Pherastar fluorescence plate reader (excitation at 340 nm, emission 520 and 490 nm; 100 ms lag time, 200 ms integration time, emission ratio = Em520/Em 490).

Alternatively, HEK293T cells were maintained in DMEM and supplements (Invitrogen). Cells were seeded at 4000000 cells per well in a 12-well plate and incubated with or without compound. After 16 h cells were treated with anisomycin (50−100 nM) (MP Biomedicals) for 5−10 min. Levels of phospho-c-Jun were measured using the phospho-c-Jun Whole Cell Lysate Kit (Meso Scale K151CGD) from Meso Scale Discovery (Gaithersburg, MD). The assay was performed according to the manufacturer's instructions, with duplicates of 10 μg of total protein from either HEK293T or C57/B6 liver cells.

THP-1 Cell Assay for Inhibition of LPS-Induced TNF-α and IL-1β Production. THP-1 cells (ATCC TIB 202, ATCC, Rockville, MD) were maintained at 37 °C, 5% CO_2 in 10% fetal bovine serum (FBS)/RPMI 1640 medium. The day of the assay, 2×10^6 cells were resuspended in 1 mL of 3% FBS/RPMI 1640 medium and plated in a 12-well plate. **19** and **11**, 12.5 μM each, or DMSO vehicle was added to the cell mixture and allowed to preincubate for 60 min at 37 °C, 5% CO_2, prior to stimulation with LPS (Sigma L6529, from *Escherichia coli* serotype 055:B5; 1 μg/mL final). LPS stimulation was allowed to proceed for 5 h at 37 °C, 5% CO_2. TNF-α and IL-1β production was measured directly from cell culture medium by a commercially available sandwich immunoassay developed by Meso Scale Discovery (Meso Scale no. K15025B-1, Gaithersburg, MD). Levels of TNF-α and IL-1β in the cell culture medium were determined using a Meso Scale Discovery Sector Imager 2400 according to the manufacturer's instructions.

Molecular Modeling. Computational docking studies were performed with GOLD 2.1 (The Cambridge Crystallographic Data Centre, Cambridge, UK)[48,49] and analyzed with Sybyl (Tripos, St. Louis). Molecular surfaces were generated with MOLCAD.[50] The X-ray coordinates of JNK1/**20**/**21** (PDB-ID 1UKI) were used to dock the compounds. Peptide and **8** and bidentate **9** poses reported in Figure 1 of the manuscript correspond to those obtained directly from the X-ray coordinates.

Glucose Tolerance Test. Male NONcNZO10/LtJ mice, 26 weeks old, from Harlan (Jackson Laboratories, Bar Harbor, Maine 04609, United States) were dosed intraperitoneally (ip) with 25 mg/kg of **19** and **11** daily for five days. Mice were fasted 16 h before ip administration of 2 g/kg D-glucose. Blood samples were taken at designated time points, and blood glucose levels were measured using a hand-held glucose meter (OneTouch Ultra, LifeScan, a Johnson & Johnson company, UK).

Liver Injury. Female C57/B6 mice, 7 weeks old, from Harlan were dosed ip with 25 mg/kg of **19**, while control mice were be treated with the vehicle only ($n = 4$). One hour later, mice were injected ip daily for three days with 0.2 μg/gram Jo-2 antibody (Fas/APO-1; BD Biosciences, catalogue no. 554255). Serum and liver were collected 4 h hence. AST and ALT levels in serum are determined using the IDEXX VetTest Chemistry Analyzer per manufacturer instructions.

Chemistry. All anhydrous solvents were commercially obtained and stored in Sure-seal bottles under nitrogen. All other reagents and solvents were purchased as the highest grade available and used without further purification. Thin-layer chromatography (TLC) analysis of reaction mixtures was performed using Merck silica gel 60 F254 TLC plates and visualized using ultraviolet light. ^{1}H NMR data were collected using a 300 MHz Varian instrument and recorded in deuteron-chloroform ($CDCl_3$) or dimethyl sulfoxide-d_6 (DMSO-d_6). Chemical shifts (δ) are reported in parts per million (ppm) referenced to ^{1}H (Me_4Si at 0.00). Mass spectral data were acquired on a Shimadzu LCMS-2010EV for low resolution, and on an Agilent ESI-TOF for high resolution and low resolution. List of Abbreviations: equivalent (eqv), high performance liquid chromatography (HPLC), liquid chromatography/mass spectrometry (LC/MS), room temperature (rt). Purity of compounds was obtained in a HPLC Breeze from Waters Co. using an Atlantis T3 3 μm 4.6 mm × 150 mm reverse phase column. All intermediate compounds were >95% pure. Following the scheme reported in Figure 1: **1** (indazole) was commercially available, which was iodinated according to the reported procedures.

Synthesis of 19. **18** was coupled with a peptide of D-amino acids on resin using standard peptide coupling conditions. After coupling reaction complete, resin was removed with the treatment of TFA. Final compound was purified by rev phase HPLC. The compound was dried and checked purity again with HPLC (purity was >93%) and analyzed with MALDI-mass. Please see Supporting Information file for HPLC trace and MALDI-Mass.

Synthesis of 3-Iodo-1-((2-(trimethylsilyl)ethoxy)methyl)-1*H*-indazole (3). To a solution of **2** (1.22 g, 5 mmol) in DMF (10 mL) was added NaH (220 mg, 5.50 mmol) in three portions at 0 °C under nitrogen atmosphere. The reaction mixture was stirred at the same temperature for 30 min, and then SEM-Cl (0.9 mL, 5 mmol) was added dropwise to it. The resulting reaction mixture was stirred at 0 °C for 1 h then at room temperature for 4 h. The reaction mixture was quenched with cold water (100 mL), followed by extraction with ether (3 × 100 mL). The combined organic layers were washed with water (100 mL) and brine (100 mL), dried ($MgSO_4$), and concentrated in vacuo. The residue was chromatographed over silica gel (5% ethyl acetate in hexane) to afford the colorless oil **3** (1.68 g, 90%), HPLC purity >95%. ^{1}H NMR (300 MHz, $CDCl_3$) δ −0.07 (s, 9 H), 0.88 (t, J = 7.2 Hz, 2 H), 3.57 (t, J = 7.5 Hz, 2 H), 5.72 (s, 2 H), 7.27 (d, J = 8.2 Hz,

1 H), 7.44−7.58 (m, 3 H). HRMS calcd for $C_{13}H_{19}IN_2OSi$ 374.0311, found 374.0312.

Synthesis of Methyl-4-(1-((2-(trimethylsilyl)ethoxy)-methyl-1*H*-indazol-3yl)benzoate (4). A mixture of **3** (374 mg, 1 mmol), 4-methoxycarbonylphenyl boronic acid (271 mg, 1.5 mmol), Pd(dppf)Cl_2 (82 mg, 0.1 mmol), saturated aqueous Na_2CO_3 solution (4 mL), in ethanol (1 mL) and toluene (10 mL) was stirred at 80 °C for 12 h. Upon completion of the reaction (TLC), the reaction mixture was extracted with CH_2Cl_2 (3 × 50 mL). The combined organic layers were washed with water (50 mL) and brine (50 mL), dried ($MgSO_4$), and concentrated in vacuo. The residue was chromatographed over silica gel (5−10% ethyl acetate in hexane) to yield the pure product **4** (295 mg, 77%), HPLC purity >96%. ^{1}H NMR (300 MHz, $CDCl_3$) δ −0.05 (s, 9 H), 0.88 (t, J = 8.4 Hz, 2 H), 3.60 (t, J = 8.4 Hz, 2 H), 3.95 (s, 3 H), 5.81 (s, 2 H), 7.28 (t, J = 7.2 Hz, 1 H), 7.42 (t, J = 7.5 Hz, 1 H), 7.62 (d, J = 8.4 Hz, 1 H), 7.85−8.22 (m, 5 H); EIMS m/z 383 $(M + H)^+$, 325, 267, 265, 149, 121, 83. HRMS calcd for $C_{21}H_{27}N_2O_3Si$ 383.1785, found 383.1784.

Synthesis of 4-(1-((2-(Trimethylsilyl)ethoxy)methyl)-1*H*-indazol-3-yl)benzoic Acid (5). To a solution of **4** (282 mg, 0.738 mmol) in THF (6 mL) and methanol (1 mL) was added LiOH solution (177 mg, 7.380 mmol) in water (2 mL). The resulting reaction mixture was stirred at room temperature for 18 h. The reaction mixture was acidified with 1 N HCl, followed by extraction with CH_2Cl_2 (3 × 50 mL). The combined organic layers were dried ($MgSO_4$) and concentrated in vacuo. The residue was chromatographed over silica gel (20−30% ethyl acetate in hexane) to afford the acid **5** (195 mg, 90%), HPLC purity >95%. ^{1}H NMR (300 MHz, $CDCl_3$) δ −0.06 (s, 9 H), 0.92 (t, J = 8.4 Hz, 2 H), 3.64 (t, J = 8.4 Hz, 5.83 (s, 2 H), 7.32 (t, J = 7.2 Hz, 1H), 7.49 (t, J = 7.5 Hz, 1 H), 7.66 (d, J = 8.4 Hz, 1 H), 8.06 (d, J = 8.4 Hz, 1 H), 8.12 (d, J = 8.7 Hz, 2 H), 8.27 (d, J = 8.1 Hz, 2 H). EIMS m/z 369 $(M + H)^+$, 339, 311, 251, 149, 121, 99, 55. HRMS calcd for $C_{20}H_{25}N_2O_3Si$ 369.1629 (M + H), found 369.1627.

Synthesis of *tert*-Butyl-3-(4-(1-((2-(trimethylsilyl)ethoxy)-methyl-1*H*-indazol-3-yl)benzamido)propylcarbamate (6). To a solution of **5** (155 mg, 0.421 mmol) in DMF (3 mL) were added EDC (96 mg, 0.505 mmol), HOBt (68 mg, 0.505 mmol), DIEA (0.19 mL, 1.052 mmol), and mono-Boc-1,3-diamino propane (82 mg, 0.463 mmol). The reaction mixture was stirred at room temperature for 16 h. Upon completion, the reaction mixture was diluted with water (40 mL), followed by extraction with ethyl acetate (3 × 40 mL). The combined organic layers were washed with saturated $NaHCO_3$ solution (2 × 30 mL), water (3 × 30 mL), and brine (30 mL) successively, dried ($MgSO_4$), and concentrated in vacuo. The residue was chromatographed over silica gel (50% ethyl acetate in hexane) to give the pure product **6** (175 mg, 79%), HPLC purity >95%. ^{1}H NMR (300 MHz, $CDCl_3$) δ −0.063 (s, 9 H), 0.91 (t, J = 8.7 Hz, 2 H), 1.47 (s, 9 H), 1.74 (quintet, J = 5.7 Hz, 2 H), 3.29 (q, J = 6 Hz, 2 H), 3.55 (q, J = 6 Hz, 2 H), 3.63 (t, J = 8.4 Hz, 2 H), 4.95 (br s, 1 H, NH), 5.80 (s, 2 H), 7.30 (d, J = 7.2 Hz, 1 H), 7.47 (t, J = 7.2 Hz, 1 H), 7.63 (d, J = 8.4 Hz, 1 H), 7.98−8.12 (m, 5 H). HRMS calcd for $C_{28}H_{40}N_4O_4Si$ 524.2819, found 524.2817.

Synthesis of *tert*-Butyl-3-(4-(1*H*-indazol-3-yl)benzamido)-propylcarbamate (7). To a solution of **6** (76 mg, 0.141 mmol) in THF (5 mL) was added TBAF (0.7 mL, 1 M solution in THF) at room temperature. The reaction mixture was refluxed for 10 h. Upon completion, the reaction mixture was partitioned between dichloromethane (40 mL) and water (30 mL). The organic layer was washed with water (30 mL) and brine (30 mL), dried ($MgSO_4$), and concentrated in vacuo. The residue was chromatographed over silica gel (80% ethyl acetate in hexane) to give the pure product **7** (42 mg, 76%), HPLC purity >95%. ^{1}H NMR (300 MHz, DMSO-d_6) δ 1.38 (s, 9 H), 1.65 (quintet, J = 6.6 Hz, 2 H), 3.01 (q, J = 6.3 Hz, 2 H), 3.30 (q, J = 6.3 Hz, 2 H), 6.83 (br s. NH), 7.24 (t, J = 7.8 Hz, 1 H), 7.42 (t, J = 6.9 Hz, 1 H), 7.62 (d, J = 8.4 Hz, 1 H),7.99 (d, J = 8.7 Hz, 2 H), 8.05−8.15 (m, 3 H), 8.52 (t, J = 5.4 Hz, 2 H), EIMS m/z 395 $(M + H)^+$, 339, 295, 221, 83. HRMS calcd for $C_{22}H_{27}N_4O_3$ 395.2078 (M + H), found 395.2077

Synthesis of *N*-(3-Aminopropyl)-4-(1*H*-indazol-3-yl)benzamide (8). To a solution of **7** (21 mg, 0.053 mmol) in CH_2Cl_2 (2 mL) was added TFA (0.5 mL). The resulting reaction mixture was stirred at room temperature for 2 h. TFA and dichloromethane were removed in vacuum to give **8**. This compound was used for the next step without further purification.

Synthesis of N^1-(1-(4-(1*H*Indazol-3-yl)phenyl-16-methyl-1,7,10,13-tetraoxo-2,6,9,12-tetraazaheptadecan-14-yl)-2(2-(2-(2-(1-(2-amino-5-guanidinopentanoyl)pyrolidine-2-carboxamido)-3-hydroxybutanamido)-3-hydroxybutanamido)-4-methylpentanamido)succinamide (9). To a solution of **8** (15 mg, 0.051 mmol) in DMF (2 mL) were added EDC (10 mg, 0.051 mmol), HOBt (6 mg, 0.051 mmol), DIEA (0.5 mL), and Boc-Arg(Pbf)-Pro-Thr(otbu)-Thr(Otbu)-Leu-Asn(trt)-Leu-Gly-Gly-OH (70 mg, 0.042 mmol) at room temperature. The reaction mixture was stirred at 50 °C for 16 h. After completion of the reaction, DMF and DIEA were removed in vacuo to give the protected compound. The crude residue was directly treated with TFA (1 mL) and H_2O (0.2 mL) for 3 h. The final product was obtained by the following HPLC purification: Atlantis Preparative T3 column (10 mm × 250 mm), acetonitrile−water system, RT = 5−34 min, yield 35%, purity >95%. ^{1}H NMR (300 MHz, CD_3OD) δ 0.74−0.79 (m, 12 H), 1.25−2.20 (m, 24 H), 2.42−2.82 (m, 2 H), 3.01−3.94 (m, 10 H), 4.10−4.65 (m, 8 H), 7.15 (br, NH), 7.34−7.45 (m, 4 H), 7.50 (br, NH), 7.61 (d, J = 8.4 Hz, 2 H), 7.74 (d, J = 7.8 Hz, 2 H), 7.89 (d, J = 8.4 Hz, 1 H), 7.95 (br, NH). EIMS m/z 1204 $(M + H)^+$, 1051, 860, 602, 450, 295, 136, 130, 108. HRMS calculated for $C_{56}H_{86}N_{17}O_{13}$ 1204.6585 (M + H), found 1204.6572.

Similarly, the synthesis of **19** was obtained by coupling methyl-4-(4-(1*H*-indazol-3-yl)benzamido) butanoate (analogue to **8** but with a free carboxylic acid in lieu of the free amine; Supporting Information) was coupled with a peptide of D-amino acids on resin using standard peptide coupling conditions. After coupling reaction complete, resin was removed with the treatment of TFA. Final compound was purified by rev phase HPLC. The compound was dried and checked purity again with HPLC (purity was >93%) and analyzed with MALDI-mass (Supporting Information).

■ ASSOCIATED CONTENT

Supporting Information. Scheme for the synthesis of and analytical data for **19**; analytical data; peptide sequences and IC_{50} values relative to their ability to displace **20**; R^2 values for various types of inhibition by **19** at either substrate or ATP binding site. This material is available free of charge via the Internet at http://pubs.acs.org.

■ AUTHOR INFORMATION

Corresponding Author

*Phone: 858-646-3159. Fax: 858-795-5225. E-mail: mpellecchia@sanfordburnham.org.

Author Contributions

‖These authors made equal contributions to this work.

■ ACKNOWLEDGMENT

Financial support was obtained by the National Institutes of Health, NIDDK branch, grant number R24DK080263. Small amounts of **19** for research purposes are available upon request.

■ ABBREVIATIONS USED

JNK, c-Jun N-terminal kinase; MAP, mitogen activated protein; MAPK, mitogen activated protein kinase; NMR, nuclear magnetic resonance spectroscopy; DELFIA, dissociation enhanced lanthanide fluoro-immuno assay; TR-FRET, time-resolved fluorescence resonance energy transfer; ALT, alanine-aminotransferase; AST, aspartate aminotransferase; TNF-α, tumor necrosis factor-α; LPS, lipopolysaccharide; IC_{50}, half-maximal inhibitory concentration; EC_{50}, half-maximal effective concentration; $K(i)$, binding affinity; ^1H NMR, ^1H nuclear magnetic resonance spectroscopy; LCMS, liquid chromatography and tandem mass spectrometry; HPLC, high-performance liquid chromatography; MALDI, matrix-assisted laser desorption/ionization; FBS, fetal bovine serum; IL-1β, interleukin 1, beta; ERK, extracellular signal-regulated kinase; ATF, cyclic AMP-dependent transcription factor; DMSO, dimethyl sulfoxide; HIV, human immunodeficiency virus; HEK, human embryonic kidney

■ REFERENCES

(1) Bogoyevitch, M. A. Therapeutic promise of JNK ATP-noncompetitive inhibitors. *Trends Mol. Med.* **2005**, *11*, 232–239.

(2) Gupta, S.; Barrett, T.; Whitmarsh, A. J.; Cavanagh, J.; Sluss, H. K.; Derijard, B.; Davis, R. J. Selective interaction of JNK protein kinase isoforms with transcription factors. *EMBO J.* **1996**, *15*, 2760–2770.

(3) Manning, A. M.; Davis, R. J. Targeting JNK for therapeutic benefit: from junk to gold? *Nature Rev Drug Discovery* **2003**, *2*, 554–565.

(4) Martin, J. H.; Mohit, A. A.; Miller, C. A. Developmental expression in the mouse nervous system of the p493F12 SAP kinase. *Brain Res. Mol. Brain Res.* **1996**, *35*, 47–57.

(5) Ip, Y. T.; Davis, R. J. Signal transduction by the c-Jun N-terminal kinase (JNK)—from inflammation to development. *Curr. Opin. Cell Biol.* **1998**, *10*, 205–219.

(6) Leppa, S.; Bohmann, D. Diverse functions of JNK signaling and c-Jun in stress response and apoptosis. *Oncogene* **1999**, *18*, 6158–6162.

(7) Minden, A.; Karin, M. Regulation and function of the JNK subgroup of MAP kinases. *Biochim. Biophys. Acta* **1997**, *1333*, F85–104.

(8) Solinas, G.; Karin, M. JNK1 and IKK{beta}: molecular links between obesity and metabolic dysfunction. *FASEB J.* **2010**, *24*, 2596–2611.

(9) Bogoyevitch, M. A.; Ngoei, K. R.; Zhao, T. T.; Yeap, Y. Y.; Ng, D. C. c-Jun N-terminal kinase (JNK) signaling: recent advances and challenges. *Biochim. Biophys. Acta* **2010**, *1804*, 463–475.

(10) Bogoyevitch, M. A.; Kobe, B. Uses for JNK: the many and varied substrates of the c-Jun N-terminal kinases. *Microbiol. Mol. Biol. Rev.* **2006**, *70*, 1061–1095.

(11) Heo, Y. S.; Kim, S. K.; Seo, C. I.; Kim, Y. K.; Sung, B. J.; Lee, H. S.; Lee, J. I.; Park, S. Y.; Kim, J. H.; Hwang, K. Y.; Hyun, Y. L.; Jeon, Y. H.; Ro, S.; Cho, J. M.; Lee, T. G.; Yang, C. H. Structural basis for the selective inhibition of JNK1 by the scaffolding protein JIP1 and SP600125. *EMBO J.* **2004**, *23*, 2185–2195.

(12) Dickens, M.; Rogers, J. S.; Cavanagh, J.; Raitano, A.; Xia, Z.; Halpern, J. R.; Greenberg, M. E.; Sawyers, C. L.; Davis, R. J. A cytoplasmic inhibitor of the JNK signal transduction pathway. *Science* **1997**, *277*, 693–696.

(13) Barr, R. K.; Kendrick, T. S.; Bogoyevitch, M. A. Identification of the critical features of a small peptide inhibitor of JNK activity. *J. Biol. Chem.* **2002**, *277*, 10987–10997.

(14) Ho, D. T.; Bardwell, A. J.; Abdollahi, M.; Bardwell, L. A docking site in MKK4 mediates high affinity binding to JNK MAPKs and competes with similar docking sites in JNK substrates. *J. Biol. Chem.* **2003**, *278*, 32662–32672.

(15) Borsello, T.; Clarke, P. G.; Hirt, L.; Vercelli, A.; Repici, M.; Schorderet, D. F.; Bogousslavsky, J.; Bonny, C. A peptide inhibitor of c-Jun N-terminal kinase protects against excitotoxicity and cerebral ischemia. *Nature Med.* **2003**, *9*, 1180–1186.

(16) Bonny, C.; Oberson, A.; Negri, S.; Sauser, C.; Schorderet, D. F. Cell-permeable peptide inhibitors of JNK: novel blockers of beta-cell death. *Diabetes* **2001**, *50*, 77–82.

(17) Kim, J. A.; Lee, J.; Margolis, R. L.; Fotedar, R. SP600125 suppresses Cdk1 and induces endoreplication directly from G2 phase, independent of JNK inhibition. *Oncogene* **2010**, *29*, 1702–1716.

(18) Bain, J.; McLauchlan, H.; Elliott, M.; Cohen, P. The specificities of protein kinase inhibitors: an update. *Biochem. J.* **2003**, *371*, 199–204.

(19) Bain, J.; Plater, L.; Elliott, M.; Shpiro, N.; Hastie, C. J.; McLauchlan, H.; Klevernic, I.; Arthur, J. S.; Alessi, D. R.; Cohen, P. The selectivity of protein kinase inhibitors: a further update. *Biochem. J.* **2007**, *408*, 297–315.

(20) Siddiqui, M. A.; Reddy, P. A. Small molecule JNK (c-Jun N-terminal kinase) inhibitors. *J. Med. Chem.* **2010**, *53*, 3005–3012.

(21) Vazquez, J.; De, S. K.; Chen, L. H.; Riel-Mehan, M.; Emdadi, A.; Cellitti, J.; Stebbins, J. L.; Rega, M. F.; Pellecchia, M. Development of Paramagnetic Probes for Molecular Recognition Studies in Protein Kinases. *J. Med. Chem.* **2008**, *51*, 3460–3465.

(22) Shuker, S. B.; Hajduk, P. J.; Meadows, R. P.; Fesik, S. W. Discovering high-affinity ligands for proteins: SAR by NMR. *Science* **1996**, *274*, 1531–1534.

(23) Jahnke, W.; Blommers, M. J.; Fernandez, C.; Zwingelstein, C.; Amstutz, R. Strategies for the NMR-based identification and optimization of allosteric protein kinase inhibitors. *ChemBioChem* **2005**, *6*, 1607–1610.

(24) Murray, B. W.; Bennett, B. L.; Sasaki, D. T. Analysis of pharmacologic inhibitors of Jun N-terminal kinases. *Methods Enzymol.* **2001**, *332*, 432–452.

(25) Enkvist, E.; Lavogina, D.; Raidaru, G.; Vaasa, A.; Viil, I.; Lust, M.; Viht, K.; Uri, A. Conjugation of adenosine and hexa-(D-arginine) leads to a nanomolar bisubstrate-analog inhibitor of basophilic protein kinases. *J. Med. Chem.* **2006**, *49*, 7150–7159.

(26) Hill, Z. B.; Perera, B. G.; Maly, D. J. A chemical genetic method for generating bivalent inhibitors of protein kinases. *J. Am. Chem. Soc.* **2009**, *131*, 6686–6688.

(27) Lavogina, D.; Enkvist, E.; Uri, A. Bisubstrate inhibitors of protein kinases: from principle to practical applications. *ChemMedChem* **2010**, *5*, 23–34.

(28) Lee, J. H.; Kumar, S.; Lawrence, D. S. Stepwise combinatorial evolution of Akt bisubstrate inhibitors. *ChemBioChem* **2008**, *9*, 507–509.

(29) Pflug, A.; Rogozina, J.; Lavogina, D.; Enkvist, E.; Uri, A.; Engh, R. A.; Bossemeyer, D. Diversity of bisubstrate binding modes of adenosine analogue−oligoarginine conjugates in protein kinase a and implications for protein substrate interactions. *J. Mol. Biol.* **2010**, *403*, 66–77.

(30) Fischer, P. M. The design, synthesis and application of stereochemical and directional peptide isomers: a critical review. *Curr. Protein Pept. Sci.* **2003**, *4*, 339–356.

(31) Shah, M.; Stebbins, J. L.; Dewing, A.; Qi, J.; Pellecchia, M.; Ronai, Z. A. Inhibition of Siah2 ubiquitin ligase by vitamin K3 (menadione) attenuates hypoxia and MAPK signaling and blocks melanoma tumorigenesis. *Pigm. Cell Melanoma Res.* **2009**, *22*, 799–808.

(32) Davies, S. P.; Reddy, H.; Caivano, M.; Cohen, P. Specificity and mechanism of action of some commonly used protein kinase inhibitors. *Biochem. J.* **2000**, *351*, 95–105.

(33) Robers, M. B.; Horton, R. A.; Bercher, M. R.; Vogel, K. W.; Machleidt, T. High-throughput cellular assays for regulated posttranslational modifications. *Anal. Biochem.* **2008**, *372*, 189–197.

(34) Comalada, M.; Xaus, J.; Valledor, A. F.; Lopez-Lopez, C.; Pennington, D. J.; Celada, A. PKC epsilon is involved in JNK activation that mediates LPS-induced TNF-alpha, which induces apoptosis in macrophages. *Am. J. Physiol. Cell Physiol.* **2003**, *285*, C1235–C1245.

(35) Baldassare, J. J.; Bi, Y.; Bellone, C. J. The role of p38 mitogen-activated protein kinase in IL-1 beta transcription. *J. Immunol.* **1999**, *162*, 5367–5373.

(36) Solinas, G.; Vilcu, C.; Neels, J. G.; Bandyopadhyay, G. K.; Luo, J. L.; Naugler, W.; Grivennikov, S.; Wynshaw-Boris, A.; Scadeng, M.; Olefsky, J. M.; Karin, M. JNK1 in hematopoietically derived cells contributes to diet-induced inflammation and insulin resistance without affecting obesity. *Cell Metab.* **2007**, *6*, 386–397.

(37) Cho, Y. R.; Kim, H. J.; Park, S. Y.; Ko, H. J.; Hong, E. G.; Higashimori, T.; Zhang, Z.; Jung, D. Y.; Ola, M. S.; Lanoue, K. F.; Leiter, E. H.; Kim, J. K. Hyperglycemia, maturity-onset obesity, and insulin resistance in NONcNZO10/LtJ males, a new mouse model of type 2 diabetes. *Am. J. Physiol. Endocrinol. Metab.* **2007**, *293*, E327–336.

(38) Kaoud, T. S.; Mitra, S.; Lee, S.; Taliaferro, J.; Cantrell, M.; Linse, K. D.; Van Den Berg, C. L.; Dalby, K. N. Development of JNK2-Selective Peptide Inhibitors That Inhibit Breast Cancer Cell Migration. *ACS Chem. Biol.* **2011**, *6*, 658–666.

(39) Maeda, S.; Chang, L.; Li, Z. W.; Luo, J. L.; Leffert, H.; Karin, M. IKKbeta is required for prevention of apoptosis mediated by cell-bound but not by circulating TNFalpha. *Immunity* **2003**, *19*, 725–737.

(40) Wang, Y.; Singh, R.; Lefkowitch, J. H.; Rigoli, R. M.; Czaja, M. J. Tumor necrosis factor-induced toxic liver injury results from JNK2-dependent activation of caspase-8 and the mitochondrial death pathway. *J. Biol. Chem.* **2006**, *281*, 15258–15267.

(41) Malhi, H.; Gores, G. J. Cellular and molecular mechanisms of liver injury. *Gastroenterology* **2008**, *134*, 1641–1654.

(42) Stebbins, J. L.; De, S. K.; Machleidt, T.; Becattini, B.; Vazquez, J.; Kuntzen, C.; Chen, L. H.; Cellitti, J. F.; Riel-Mehan, M.; Emdadi, A.; Solinas, G.; Karin, M.; Pellecchia, M. Identification of a new JNK inhibitor targeting the JNK-JIP interaction site. *Proc. Natl. Acad. Sci. U.S.A* **2008**, *105*, 16809–16813.

(43) De, S. K.; Chen, V.; Stebbins, J. L.; Chen, L. H.; Cellitti, J. F.; Machleidt, T.; Barile, E.; Riel-Mehan, M.; Dahl, R.; Yang, L.; Emdadi, A.; Murphy, R.; Pellecchia, M. Synthesis and optimization of thiadiazole derivatives as a novel class of substrate competitive c-Jun N-terminal kinase inhibitors. *Bioorg. Med. Chem.* **2010**, *18*, 590–596.

(44) De, S. K.; Chen, L. H.; Stebbins, J. L.; Machleidt, T.; Riel-Mehan, M.; Dahl, R.; Chen, V.; Yuan, H.; Barile, E.; Emdadi, A.; Murphy, R.; Pellecchia, M. Discovery of 2-(5-nitrothiazol-2-ylthio)benzo[*d*]thiazoles as novel c-Jun N-terminal kinase inhibitors. *Bioorg. Med. Chem.* **2009**, *17*, 2712–2717.

(45) De, S. K.; Stebbins, J. L.; Chen, L. H.; Riel-Mehan, M.; Machleidt, T.; Dahl, R.; Yuan, H.; Emdadi, A.; Barile, E.; Chen, V.; Murphy, R.; Pellecchia, M. Design, synthesis, and structure−activity relationship of substrate competitive, selective, and in vivo active triazole and thiadiazole inhibitors of the c-Jun N-terminal kinase. *J. Med. Chem.* **2009**, *52*, 1943–1952.

(46) Caelles, C.; Morales, M. Assays to measure stress-activated MAPK activity. *Methods Mol. Biol.* **2004**, *282*, 145–156.

(47) Huwiler, K. G.; Machleidt, T.; Chase, L.; Hanson, B.; Robers, M. B. Characterization of serotonin 5-hydroxytryptamine-1A receptor activation using a phospho-extracellular-signal regulated kinase 2 sensor. *Anal. Biochem.* **2009**, *393*, 95–104.

(48) Eldridge, M. D.; Murray, C. W.; Auton, T. R.; Paolini, G. V.; Mee, R. P. Empirical scoring functions: I. The development of a fast empirical scoring function to estimate the binding affinity of ligands in receptor complexes. *J. Comput.-Aided Mol. Des.* **1997**, *11*, 425–445.

(49) Jones, G.; Willett, P.; Glen, R. C.; Leach, A. R.; Taylor, R. Development and validation of a genetic algorithm for flexible docking. *J. Mol. Biol.* **1997**, *267*, 727–748.

(50) Teschner, M.; Henn, C.; Vollhardt, H.; Reiling, S.; Brickmann, J. Texture mapping: a new tool for molecular graphics. *J. Mol. Graphics* **1994**, *12*, 98–105.